ARTICLES

Journal of Semiconductors
(2023) 44, 112001
doi: 10.1088/1674-4926/44/11/112001

Multilayered $PdTe_2$/thin Si heterostructures as self-powered flexible photodetectors with heart rate monitoring ability

Chengyun Dong[1], Xiang An[1], Zhicheng Wu[1], Zhiguo Zhu[1], Chao Xie[2, †], Jian-An Huang[3], and Linbao Luo[1, †]

[1]School of Microelectronics, Hefei University of Technology, Hefei 230009, China

[2]Industry-Education-Research Institute of Advanced Materials and Technology for Integrated Circuits, Information Materials and Intelligent Sensing Laboratory of Anhui Province, Anhui University, Hefei 230601, China

[3]Faculty of Medicine, Faculty of Biochemistry and Molecular Medicine, University of Oulu, 90220 Oulu, Finland

Abstract: Two-dimensional layered material/semiconductor heterostructures have emerged as a category of fascinating architectures for developing highly efficient and low-cost photodetection devices. Herein, we present the construction of a highly efficient flexible light detector operating in the visible-near infrared wavelength regime by integrating a $PdTe_2$ multilayer on a thin Si film. A representative device achieves a good photoresponse performance at zero bias including a sizeable current on/off ratio exceeding 10^5, a decent responsivity of ~343 mA/W, a respectable specific detectivity of ~2.56×10^{12} Jones, and a rapid response time of 4.5/379 μs, under 730 nm light irradiation. The detector also displays an outstanding long-term air stability and operational durability. In addition, thanks to the excellent flexibility, the device can retain its prominent photodetection performance at various bending radii of curvature and upon hundreds of bending tests. Furthermore, the large responsivity and rapid response speed endow the photodetector with the ability to accurately probe heart rate, suggesting a possible application in the area of flexible and wearable health monitoring.

Key words: 2D layered material; heterostructure; flexible; photodetector; health monitoring

Citation: C Y Dong, X An, Z C Wu, Z G Zhu, C Xie, J A Huang, and L B Luo, Multilayered $PdTe_2$/thin Si heterostructures as self-powered flexible photodetectors with heart rate monitoring ability[J]. *J. Semicond.*, 2023, 44(11), 112001. https://doi.org/10.1088/1674-4926/44/11/112001

1. Introduction

Photodetectors are a group of photoelectric devices that convert photonic signals into electrical signals and have found critical uses in many areas, including light communication, optical imaging, security and environmental monitoring, medical diagnostics apparatus and so on[1–4]. Traditionally, commercial light detection devices are manufactured with inorganic semiconductor materials (*e.g.*, crystalline Si, Si/Ge heterostructures, group Ⅲ–Ⅴ semiconductors and alloys) and have gained excellent photoresponse features in the light wavelength spectrum of visible-near infrared (NIR) regimes[2, 5, 6]. However, further development and vast applications of these devices are restricted by some existing dilemmas, including epitaxially grown photoactive materials with good crystalline quality, complex device structures, intricate multistep fabricating procedures and expensive instruments requiring fine vacuum and so on. Over the last few decades, there is an increasing interest in developing high-performance and low-cost photodetection devices by exploring novel functional materials, such as quantum dots[7, 8], nanowires[9–11], 2D layered materials[12–15], hybrid perovskite materials[16–18], and so on. As recently explored 2D layered materials, group-10 transition metal dichalcogenides (TMDs, *e.g.*, PtS_2, $PtSe_2$, $PdSe_2$, $PdTe_2$, *etc.*) have attracted extensive research attention in recent years because of their appealing physical characteristics, including large charge carrier mobilities of over 1000 $cm^2/(V\cdot s)$ in theory, layer-dependent adjustable bandgaps from 0–0.25 eV in bulk to 1.2–1.75 eV for single-layers, and prominent stability in ambient conditions[13, 19, 20]. Indeed, these prominent material features render group-10 TMDs very attractive for manufacturing broadband light detectors with photoresponse spanning from the visible to the NIR wavelength spectra[21–25].

To further boost photoresponse performance of group-10 TMD-based photodetectors, an alternative approach is to explore hybrid heterostructures that are composed of 2D group-10 TMD/traditional three-dimensional (3D) semiconductors[26–29]. Compared with a pure group-10 TMD-based device, the hybrid heterostructures may offer the following benefits: (1) improved light absorption ability and widened optical absorption spectral regime due to additional light absorption from 3D semiconductor; (2) more effective separation and transport of photoexcited charge carriers thanks to an internal electric field; (3) self-powered photodetection ability at zero bias because of the strong photovoltaic effect; and (4) exotic functionalities brought by complementary features of both components. For instance, Yim *et al*. combined $PtSe_2$ multilayer with bulk Si to construct a wideband heterojunction light detector, which possesses a maximum responsivity of 490 mA/W and relatively poor responsivity of 0.1–1.5 mA/W at photon energies above and below the Si bandgap, respectively[26]. Wu and colleagues reported a self-powered broadband photodetector composed of a

Correspondence to: C Xie, chaoxie@ahu.edu.cn; L B Luo, luolb@hfut.edu.cn

Received 20 APRIL 2023; Revised 6 JUNE 2023.

©2023 Chinese Institute of Electronics

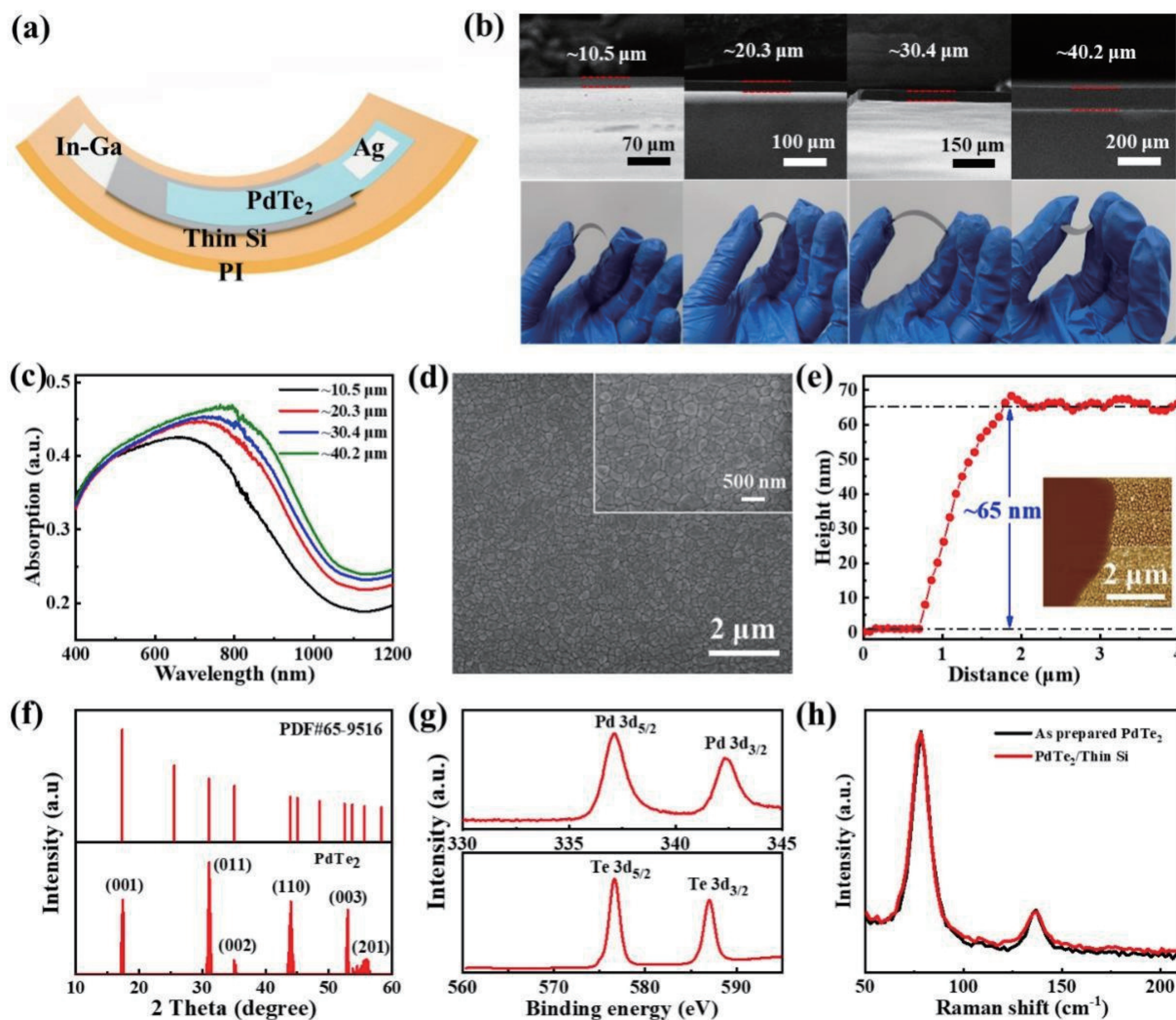

Fig. 1. (Color online) (a) Schematic diagram of the $PdTe_2$ multilayer/thin Si heterostructure-based flexible photodetector. (b) Cross-sectional SEM images (top panel) thin Si films with different thicknesses. The bottom panel shows photographs of thin Si films under bending conditions. (c) Absorption spectra of thin Si films with different thicknesses. (d) SEM images, (e) height profile, (f) XRD pattern, and (g) XPS spectra of as-prepared $PdTe_2$ multilayer. Inset in (e) displays an AFM image of the $PdTe_2$ multilayer. (h) Raman spectra of as-prepared $PdTe_2$ multilayer on a SiO_2/Si substrate and $PdTe_2$ multilayer transferred onto a thin Si film.

graphene/$PdSe_2$ multilayer/bulk Ge heterojunction[27]. Thanks to the anisotropic material properties of the $PdSe_2$, the light detector is highly polarization-sensitive with a record polarization sensitivity among 2D layered material-based photodetectors. Nevertheless, although significant achievements have been gained, the exploration of flexible photodetectors based on group-10 TMD/semiconductor heterostructures are thus far scarcely reported. Meanwhile, the development of flexible and wearable health monitoring devices is becoming increasingly important nowadays due to deterioration of the environment and increasing number of human diseases worldwide[30, 31].

In this work, by combing a $PdTe_2$ multilayer with a thin Si film, we report the construction of a flexible heterojunction photodetector, which can work in the visible-near infrared wavelength regions with outstanding photoresponse performance. At zero bias, the key performance figure-of-merits in terms of current on/off ratio, responsivity, specific detectivity and response speed can attain over 10^5, ~343 mA/W, ~2.56×10^{12} Jones, and 4.5/379 μs, respectively. In addition, the excellent photoresponse performance remains almost unchanged at different bending radii of curvature and upon hundreds of bending tests, suggesting eminent flexibility and operational durability of the device. It is also revealed that the light detector can accurately detect heart rate (HR) *via* photoplethysmography (PPG) test, which is highly desirable in a real-time health monitoring application.

2. Results and discussion

Fig. 1(a) depicts a diagrammatic sketch of the designed flexible photodetector composed of a $PdTe_2$ multilayer/thin Si heterostructure, and the detailed fabricating procedures are provided in Fig. S1. In brief, thin Si films with various thicknesses of about 10.5, 20.3, 30.2, and 40.3 μm were obtained by immersing pre-cleaned 500 μm-thick Si substrates in a KOH etchant for different etching durations of about 16, 14, 12, and 10 h, respectively, at 100 °C in ambient conditions[32]. To diminish the precipitate of silicates at the surface of Si, the substrates were taken out of the etchant, rinsed with DI water and then placed gently into another fresh etchant sequentially every 2 h in the experiments. After etching, the thin Si film was washed with deionized water and trans-

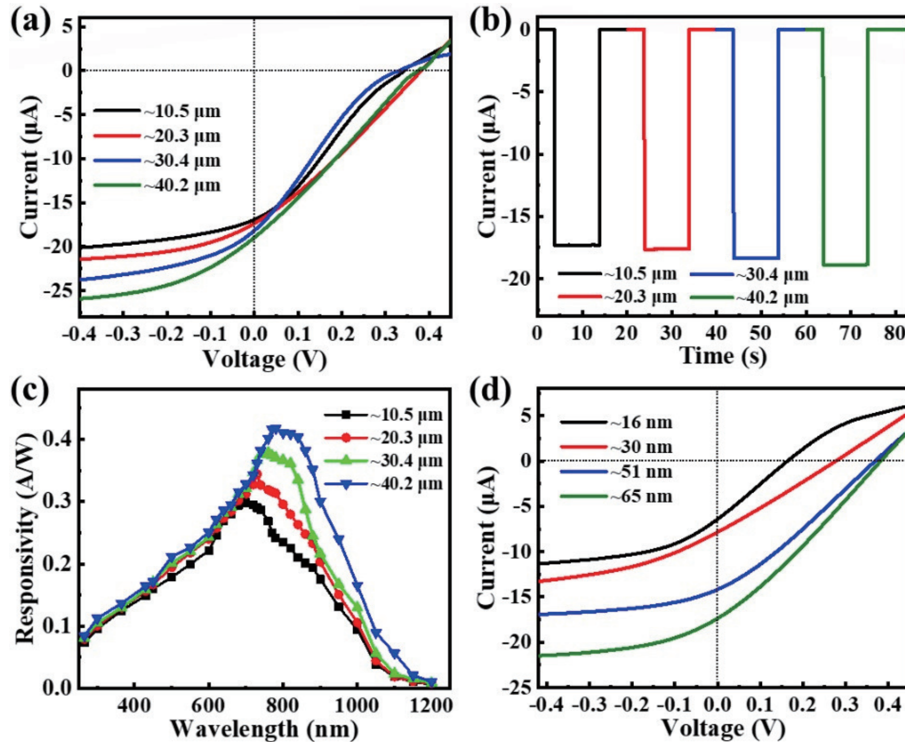

Fig. 2. (Color online) (a) *I–V* curves, (b) transient photoresponse at zero bias and (c) responsivity *versus* light wavelength of $PdTe_2$ multilayer/thin Si heterostructure with diverse Si thicknesses. (d) *I–V* curves of $PdTe_2$ multilayer/thin Si heterostructure with different $PdTe_2$ thicknesses.

ferred onto a flexible polyimide (PI) substrate. In-Ga alloy serving as Ohmic contact was daubed on the back side of the thin Si film. $PdTe_2$ multilayer was grown *via* a thermal-assisted tellurization technique using ~8 nm-thick Pd film as a precursor and transferred onto the thin Si film to form a heterostructure with the help of a wet transfer technique[33]. Afterwards, an Ag electrode with a thickness of 80 nm was fabricated by using electron beam evaporation to form Ohmic contact with $PdTe_2$. Fig. 1(b) displays the cross-sectional scanning electron microscopy (SEM) images of the fabricated thin Si films with diverse thicknesses, along with their optical images. It was seen that all thin Si films showed a very uniform thickness in a large area. In addition, all thin Si films can be readily bent, indicating a good flexibility. As expected, the flexibility increased with decreasing Si thickness. Fig. 1(c) compares the absorption spectra of thin Si films with different thicknesses, which were recorded on a UV–Vis–NIR spectrophotometer (Agilent Technologies, Cary 5000). Apparently, all thin Si films demonstrated distinct absorption of incident light spanning a broad wavelength spectrum in the range of the visible to NIR regions. With decreasing Si thickness, the photo absorption especially in the Vis–NIR ranges gradually declined, due primarily to the fact that photons with longer wavelength require thicker Si to be fully absorbed, whereas those with shorter wavelength tend to be absorbed near the surface region of Si[34]. SEM images of as-grown $PdTe_2$ multilayer on a SiO_2/Si substrate are displayed in Fig. 1(d), showing that the thermal-assisted tellurization technique could render a compact and continuous film in a large area with a relatively flat surface. The energy dispersive X-ray spectroscopy (EDS) was employed to study the elemental composition of the as-synthesized sample. As shown in Fig. S2(a), the atomic ratio of Pd/Te was determined to be 1/2.11, which approaches the stoichiometric composition of $PdTe_2$. In addition, as observed from the atomic force microscopy (AFM) image (inset in Fig. 1(e)), the $PdTe_2$ multilayer with a thickness of about 65 nm has a polycrystalline structure comprising vast dense crystalline domains with sizes ranging from about 100 to 400 nm, which is consistent with the observation from SEM images. Fig. 1(f) plots the X-ray diffraction (XRD) pattern of the as-grown $PdTe_2$ multilayer, where notable diffraction peaks at 17.4°, 31.1°, 35°, 44°, 53°, and 56° corresponded to (001), (011), (002), (110), (003), and (201) crystal planes of $PdTe_2$, respectively. No extra Pd or Te peaks were found, signifying the high phase purity of the product. The X-ray photoelectron spectroscopy (XPS) characterization was also conducted to probe the element component and binding states of the $PdTe_2$ multilayer. As plotted in Fig. 1(g), distinct peaks located at around 337, 342, 576, and 587 eV were due to the orbitals of Pd $3d_{5/2}$, Pd $3d_{3/2}$, Te $3d_{5/2}$, and Te $3d_{3/2}$, respectively[35]. Furthermore, the Raman spectra of as-prepared $PdTe_2$ multilayer on a SiO_2/Si substrate and $PdTe_2$ multilayer transferred onto a thin Si film were collected and compared (Fig. 1(h)). It was observed that, for both samples, two representative peaks at ~78.4 and ~137.1 cm^{-1} corresponding to the in-plane (E_g) and out of-plane (A_{1g}) motions of Te atoms, respectively, could be found[36]. The location and intensity of both peaks showed no obvious change. Based on these results, we confirmed that $PdTe_2$ multilayer with good quality has been successfully synthesized and the transfer process does not cause obvious damage on the $PdTe_2$ multilayer.

To select thin Si film with a more suitable thickness for assembling flexible devices, photodetectors based on $PdTe_2$ multilayer/thin Si heterostructures with diverse Si thicknesses of about 10.5, 20.3, 30.2, and 40.3 μm were constructed and investigated (the thickness of $PdTe_2$ is ~65 nm for these devices). To ensure that all devices have identical

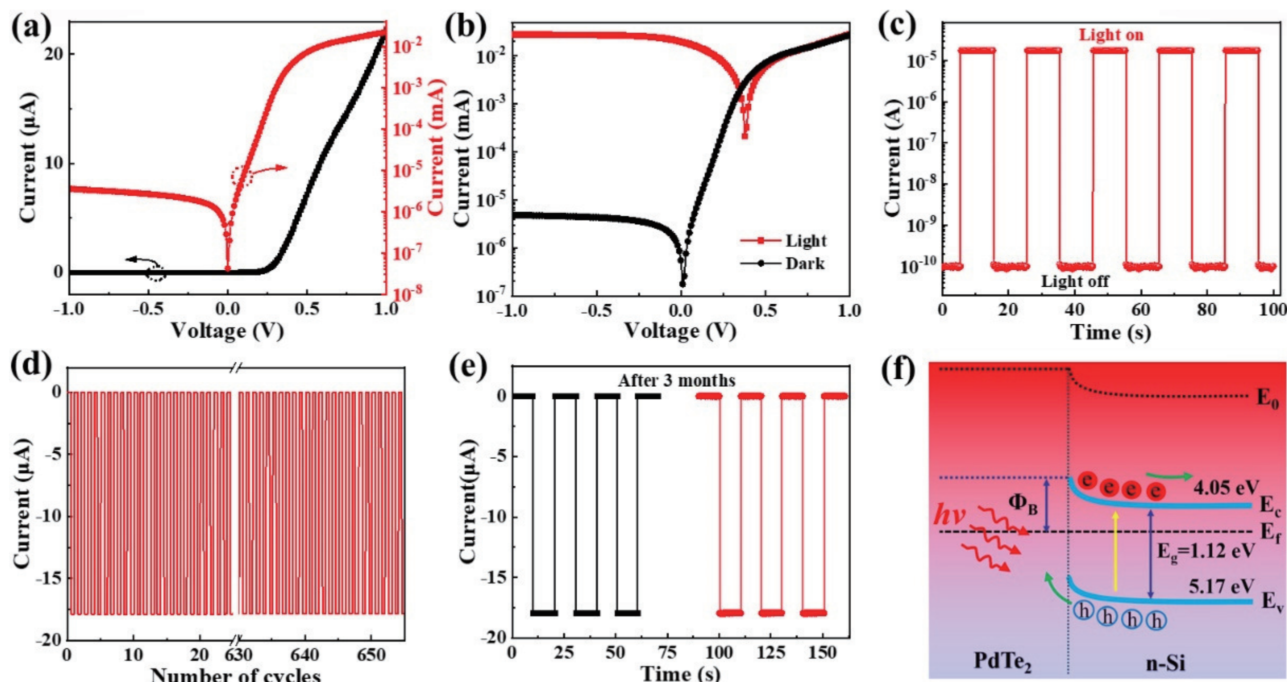

Fig. 3. (Color online) (a) Dark *I*–*V* curve of the $PdTe_2$ multilayer/thin Si heterostructure in linear and logarithmic coordinates. (b) The comparison of the *I*–*V* curves in darkness and upon 730 nm light irradiation. (c) Transient photoresponse upon periodically switched 730 nm light irradiation. Transient photoresponse (d) after over 650 cycles of working and (e) before and after storage for 3 months in air conditions. (f) Energy band diagram of the heterostructure upon light irradiation at 0 V.

effective light-receiving areas, a shadow mask with a hollow hole of approximately 0.09 cm^2 was placed between light source and photodetectors in the experiments. Figs. 2(a) and 2(b) plot the current–voltage (*I*–*V*) curves and transient photoresponse at zero bias of these devices under 730 nm light irradiation with identical intensity of around 1.06 mW/cm^2. Obviously, all devices demonstrated distinct photovoltaic behavior to incident light illumination, and could therefore function as self-powered light detectors operating at zero bias. The photocurrent at zero bias increased gradually from ~17.32, ~17.65, ~18.37, to ~18.89 μA when the thickness of thin Si was changed from ~10.5, ~20.3, ~30.2, to ~40.3 μm, respectively. Fig. 2(c) further compares the responsivity of these devices as functions of incident light wavelength from 250 to 1200 nm (the method for calculating the responsivity of a photodetector was supplied in the latter section). Significantly, all devices showed sensitive photoresponse features at wavelengths of 300–1000 nm. The values of responsivity rose gradually with increasing thin Si thickness, in particular at light wavelengths exceeding 700 nm. The peak responsivities were found to be ~298, ~344, ~378, and ~417 mA/W for the four devices, respectively. In addition, a red shift of peak responsivity located at ~700, ~730, ~760, and ~780 nm, respectively, was observed. The evolution of responsivity versus light wavelength for devices with different thin Si thicknesses was directly correlated to the distinct light absorption properties of these thin Si films (Fig. 1(c)). Specifically, it was found that these devices exhibited poorer photoresponse at 800–1200 nm NIR wavelength region as compared with commercial Si photodiodes, which should be attributed to the weakened optical absorption ability of thin Si films at this spectrum regime (Fig. 1(c)). These results imply that devices assembled on thicker Si could possess a more excellent photoresponse performance. However, considering the relatively poorer flexibility of thin Si films with thickness of ~30.2 μm and ~40.3 μm, as well as the breakable feature of ~10.5 μm-thick thin Si film during bending tests, ~20.3 μm-thick thin Si film was employed to construct flexible photodetectors in this work, and the following experiments and discussions are all based on ~20.3 μm-thick Si-based devices. In addition to thin Si thickness, the thickness of $PdTe_2$ film also has an influence on the device photoresponse performance. Fig. 3(d) and Fig. S2(b) show the *I*–*V* curves and transient photoresponse of heterostructure devices with different $PdTe_2$ thicknesses of about 16, 30, 51, and 65 nm, respectively. It was observed that the detectors exhibited gradually enhanced photovoltaic activity and increased photoresponse with increasing $PdTe_2$ thickness. This behavior should primarily be attributed to the higher electrical conductivity of thicker $PdTe_2$ film that decreased contact resistance in the light detectors (Fig. S2(c)). So, the thickness of $PdTe_2$ was optimally selected to be ~65 nm here.

Fig. 3(a) displays the dark *I*–*V* characteristic of a representative $PdTe_2$ multilayer/thin Si (~20.3 μm) heterostructure, revealing a representative current rectifying feature. This current rectifying behavior should come solely from the heterojunction formed between $PdTe_2$ and Si because of the good Ohmic contacts of Ag/$PdTe_2$/Ag and In-Ga/Si/In-Ga structures (Fig. S2(d)). The forward-to-reverse ratio could approach 10^4 within the applied voltage of ±1 V, which was superior to $PtSe_2$ multilayer/Si (~100) and WS_2 multilayer/Si (~100) heterostructures in the literature[26, 37]. Additionally, the ideality factor (*n*) of the heterostructure was calculated to be ~1.24, determined by the ln*I*–*V* characteristic shown in Fig. S3(a)[38]. Such an ideality factor closing to the value of an ideal diode (1) is superior to many similar heterostructures, including

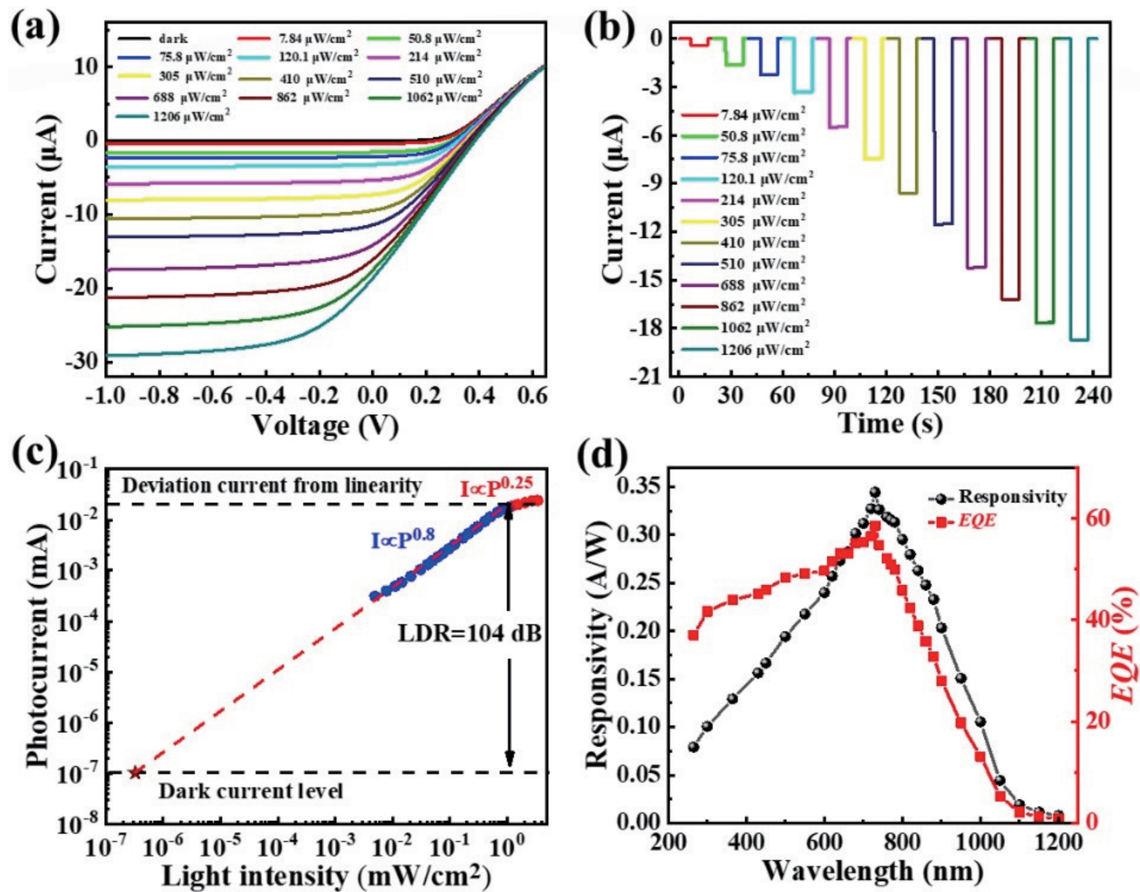

Fig. 4. (Color online) (a) I–V characteristics and (b) transient photoresponse of the heterostructure photodetector under 730 nm light irradiation with diverse intensities. (c) Photocurrent at 0 V *versus* intensity of incident light. The dark current level and deviation current from linearity determine the LDR of the light detector. (d) Dependence of responsivity and EQE on wavelength of incident light.

MoS_2 multilayer/Si (n = 1.83) and $PtTe_2$ multilayer/Si (n = 1.85)[39, 40]. Furthermore, according to the theory of thermionic emission, the barrier height was calculated to be ~827 meV for this heterostructure (Fig. S3(b)), which surpassed the values of heterostructures of few-layered $PtSe_2$/Si (~710 meV) and graphene/Si (~450 meV)[26, 41]. These results signify the realization of a heterostructure with high-quality.

The comparison of the I–V curves in darkness and upon light illumination is plotted in Fig. 3(b). Clearly, under 730 nm light irradiation possessing an intensity of about 1.5 mW/cm^2, the heterostructure exhibited an obvious photovoltaic behavior with short circuit current and open circuit voltage of about 19.96 μA and 0.38 V, respectively. The transient photoresponse upon periodically switched light illumination (~1.06 mW/cm^2) was further studied, as demonstrated in Fig. 3(c). It was observed that the current could closely follow the rapidly changing light signal, rendering repeatable and reversible high- and low-current statues with a sizable current on/off ratio attaining about 1.5 × 10^5. It was also noted that the heterostructure device could quickly separate and collect the photogenerated charge carriers and also held a rapid response speed, as evidenced by the sharp rise and fall edges in the transient photoresponse curve. Additionally, the present light detector possessed excellent operational stability and durability in ambient circumstances. Figs. 3(d) and 3(e) display the transient photoresponse after over 650 cycles of operation and before and after storage for 3 months in air circumstances, respectively. One can see that both photocurrent and dark current maintained their initial values with negligible degradation. Therefore, the light detector could well maintain its prominent photo-switching characteristics.

Fig. 3(f) illustrates the energy band diagram of the $PdTe_2$ multilayer/thin Si heterostructure, from which the physical mechanism of the above observed self-powered photoresponse behavior could be understood. The work function values are ~4.80 and ~4.25 eV for the $PdTe_2$ multilayer featuring semi-metallic nature and the n-Si having a resistivity of 1–10 Ω/cm, respectively[33]. In case the two materials contacted with each other, the difference in work functions led to diffusion of electrons from n-Si to $PdTe_2$ up to attaining the thermal equilibrium state, which rendered the bending of the energy levels in the depletion region and the formation of an internal electric field at heterostructure interface[42]. While the device was exposed to light irradiation holding photon energy higher than the bandgap of Si (1.12 eV), pairs of electrons and holes would be excited in the heterostructure. Electrons and holes within or near the depletion region were rapidly separated by the strong internal electric field. Immediately, the electrons transferred across the thin Si film and gathered by the bottom In-Ga contact, and the holes passed through the $PdTe_2$ and reached the Ag contact, producing a sizeable photocurrent at zero bias.

We noted that such a self-powered photodetection characteristic relied strongly on the intensity of the incident light. Fig. 4(a) displays the I–V curves in dark and under 730 nm light irradiation with diverse intensities for the device. Appar-

ently, both the photovoltage and photocurrent at reverse and zero biases were raised with an increase in the light intensity. Specifically, the photocurrent at 0 V could rise from ~0.39 μA when the light changed intensity from about 7.84 $\mu W/cm^2$ to 1.21 mW/cm^2. The transient photoresponse upon diverse light intensities was also explored and is shown in Fig. 4(b). It was observed that the transient photoresponse had the identical tendency as found in the I–V characteristics when changing the light intensity, and the light detector exhibited good photo-switching properties under various light illuminating conditions covering a wide intensity range. Generally, such a relationship between photocurrent and light intensity can be fitted by an extensively employed formula: $I_{ph} \propto P^{\theta}$, where I_{ph} and P represent the photocurrent and the intensity of incident light, respectively, and θ denotes an empirical value relating to the activity of photocarrier recombination[39]. As displayed in Fig. 4(c), fitting the curve of photocurrent at 0 V as a function of light intensity gave a large θ value of 0.8 approaching the ideal value of 1 at a low light intensity regime of 7.84 $\mu W/cm^2$–1.06 mW/cm^2 and a non-ideal value of 0.25 at a high light intensity region of 1.21–3.4 mW/cm^2, respectively. Thus, it could be inferred that the photocurrent loss owing to charge carrier recombination was weak at lower light intensity and became severe at higher light intensity[38]. The low light intensity region of 7.84 $\mu W/cm^2$–1.06 mW/cm^2 was within the linear dynamic range (LDR) of the light detector, and the photocurrent at 1.21 mW/cm^2 light intensity became deviation from the LDR of the device. Furthermore, by extrapolating to the dark current level (~10^{-10} A), the LDR of this device was deduced to be about 104 dB, according to the formula: LDR = $20\log(I^{*}_{ph}/I_{dark})$, where I^{*}_{ph} and I_{dark} represented the photocurrent deviating from linearity and dark current level, respectively[43]. This value was slightly lower than a commercial Si-based photodiode (120 dB) and could meet most application scenarios of photodetectors[44].

To facilitate a comparison of the photoresponse performance of different light detectors, two pivotal performance figure-of-merits, *e.g.*, responsivity (R) and external quantum efficiency (EQE) were then studied based on the following equation[12]:

$$R = \frac{I_{ph}}{SP} = G\left(\frac{q\lambda}{hc}\right)\mathrm{EQE}, \tag{1}$$

where S, G, q, λ, h, and c denote the effective device area (~0.09 cm^2), photocurrent gain, elementary charge, incident light wavelength, Planck's constant, and speed of light, respectively. The G can be considered as 1 in a normal photovoltaic-type detector absence of an internal gain mechanism[42]. Accordingly, the maximum R and EQE could attain approximately 343 mA/W and 58.6%, respectively, upon 730 nm light irradiation at zero bias. The sizable R value was comparable to many light detectors comprising 2D layered material/Si heterostructures, including graphene/Si (435 mA/W at −2 V), MoS_2/Si (~300 mA/W at 0 V) and $PtSe_2$/Si (490 mA/W at 0 V)[26, 39, 41]. In light of the relatively lower optical absorption because of reduced thickness in thin Si film, the R and EQE could be further enhanced by introducing anti-reflection techniques, such as employing light-trapping pyramid-Si structure[45]. The dependencies of R and EQE on incident light wavelength were further investigated and are displayed in Fig. 4(d). We found that the present light detector held a sensitive photoresponse feature over a broad wavelength spectrum of 300–1000 nm with a peak response at around 730 nm.

The ability to sense weak light signals is critical for a photodetector, which is described by specific detectivity (D^*), as well as noise equivalent power (NEP). The two performance parameters are usually expressed as follows[46]:

$$D^{*} = \frac{(S\Delta f)^{1/2}}{\mathrm{NEP}}, \tag{2}$$

$$\mathrm{NEP} = \frac{\overline{i_n^2}^{1/2}}{R}, \tag{3}$$

where Δf and $\overline{i_n^2}^{1/2}$ represent the bandwidth and the root-mean-square value of the noise current, respectively. By doing Fourier transform of dark current recorded at zero bias, the $\overline{i_n^2}^{1/2}$ at the bandwidth of 1 Hz was estimated to be ~4.0×10^{-14} $AHz^{-1/2}$ (Figs. S3(c) and (d)). Thus, the NEP was deduced to be ~1.17×10^{-13} $WHz^{-1/2}$, giving a respectable D^* of approximately 2.56×10^{12} Jones at zero bias.

We also examined the response speed of this device, which reflected its capability to detect rapidly varying optical signals. Fig. 5(a) plots the transient photoresponse upon 730 nm light irradiation with different modulated frequencies. It was found that although the photoresponse experienced somewhat of a decline with an increase in modulated frequency, the light detector could still exhibit a reversible and repeatable photoresponse with stable photo-switching characteristics, even at a large frequency of 5000 Hz. From the curve of relative balance $(V_{max}-V_{min})/V_{max}$ *versus* modulated frequency (Fig. 5(b)), the 3dB frequency described as the frequency where the photoresponse dropped to 0.707 of the maximum photoresponse value was estimated to be about 994 Hz[47]. In addition, as observed in Fig. 5(c), the rise and fall times of response speed were determined to be 4.5 and 379 μs, respectively, which were comparable to many 2D layered material/Si heterostructure-based light detectors in the literature[14, 42]. The comparable or even shorter rise time was due primarily to the thin thickness of Si used here, compared with most bulk Si-based devices (Table 1). The ~20.3 μm-thick thin Si film greatly shortened the distance that photocarriers need to transport through from Si to bottom electrode, giving rise to a shorter transition time and therefore a faster rising speed. Meanwhile, the relatively longer fall time here was probably caused by the complicated recombination activities of photogenerated carriers after turning off the light illumination. The residual silicates on the surface of thin Si during its preparation in KOH etchantserve as recombination centers to trap and de-trap photoexcited charge carriers, causing a longer fall time in response speed[48]. Table 1 summarizes the key performance parameters of the previously reported 2D material/Si heterostructure-based photodetectors with our device for comparison.

The excellent flexibilities of the ~20.3 μm-thick Si film and the $PdTe_2$ multilayer enabled the present heterostruc-

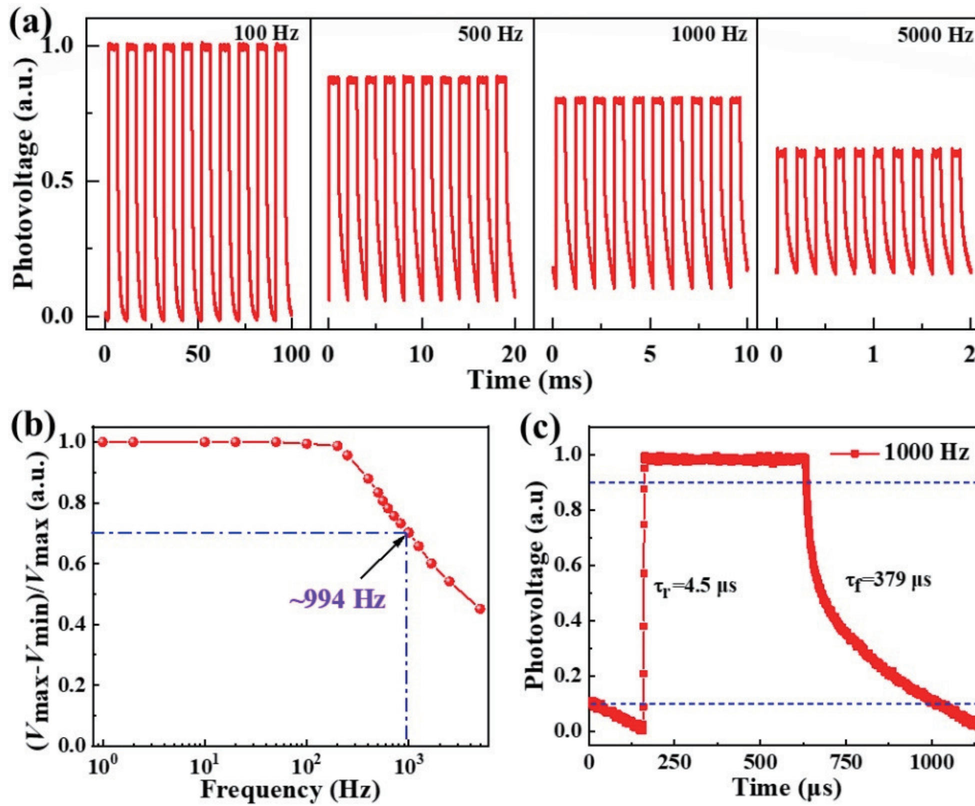

Fig. 5. (Color online) (a) Transient photoresponse upon 730 nm light irradiation with various modulated frequencies. (b) Relative balance (V_{max} – V_{min})/V_{max} *versus* incident light frequency, showing a 3 dB frequency at about 994 Hz. (c) An individual cycle transient photoresponse.

Table 1. Comparison of key performance parameters of previously reported 2D material/Si heterostructure-based photodetectors with our device.

Device structure	R (mA/W)	D^* (Jones)	Rise/fall time (μs)	Ref.
$PdSe_2$/bulk Si	300.2 (0 V)	~10^{13}	38/44	[28]
WS_2/bulk Si	224 (0 V)	1.5×10^{12}	16/29	[37]
MoS_2/bulk Si	~300 (0 V)	~10^{13}	3/40	[39]
$PtTe_2$/bulk Si	428 (0 V)	5.89×10^{11}	2.4/32	[40]
Graphene/bulk Si	435 (-2 V)	7.69×10^{9}	1200/3000	[41]
$PdTe_2$/thin Si	343 (0 V)	~2.56×10^{12}	4.5/379	This work

ture to function as a flexible light detector. In this experiment, opposite sides of the PI substrate employed to fabricate the flexible device were fixed by using a vernier caliper, which could adjust the deformation degree of the substrate to attain various bending radii of curvature. Fig. 6(a) plots the *I–V* characteristics in darkness and upon 730 nm light irradiation at different bending radii of curvature of ∞ (flat status), 0.65, 0.73, 0.85, 0.95, and 1.35 cm. The corresponding photocurrent and dark current derived from transient photoresponses are also presented in Fig. 6(b). It can be seen that despite some weak fluctuations in dark current, the photocurrent stayed almost unchanged, suggesting that the present light detector could maintain its good photo-switching properties and operate well at different bending conditions. In addition, the photoresponse properties were also explored after hundreds of bending tests at a fixed bending radius of curvature of 0.85 cm. As displayed in Figs. 6(c) and 6(d), the photocurrent showed negligible change, while the dark current even experienced somewhat of a decline after 100 and 200 cycles of bending tests, signifying the robust stability of the light detector under repetitive mechanical bending. The fluctuation or decline in dark current might be caused by the slight variation in contact between thin Si film and In-Ga electrode when bending. These results unambiguously reveal the outstanding flexibility and operational durability of the $PdTe_2$ multilayer/thin Si heterostructure-based flexible photodetector.

The collective features of the present heterostructure-based light detector, *e.g.*, the sizeable photoresponse spanning the absorption spectrum of hemoglobin and also the short response times, afforded it the ability to serve as a photoplethysmography (PPG) sensor for HR detection[49, 50]. Figs. 7(a) and 7(b) give a schematic diagram and the experimental setup for HR detection using this device, respectively. A 730 nm light beam was transmitted through the finger tissue of a volunteer and reached the underlying light detector. During cardiac cycles, the alteration of blood-volume in the veins was converted to pulsatile signals collected by a SourceMeter, from which the HR data could be extracted. Figs. 7(c) and 7(d) present the obtained pulse PPG signals of the volunteer at normal and immediately after exercise statuses, respectively. The HRs at the two conditions were deduced to be 70.8 and 118.8 beats/min, respectively, *via* divid-

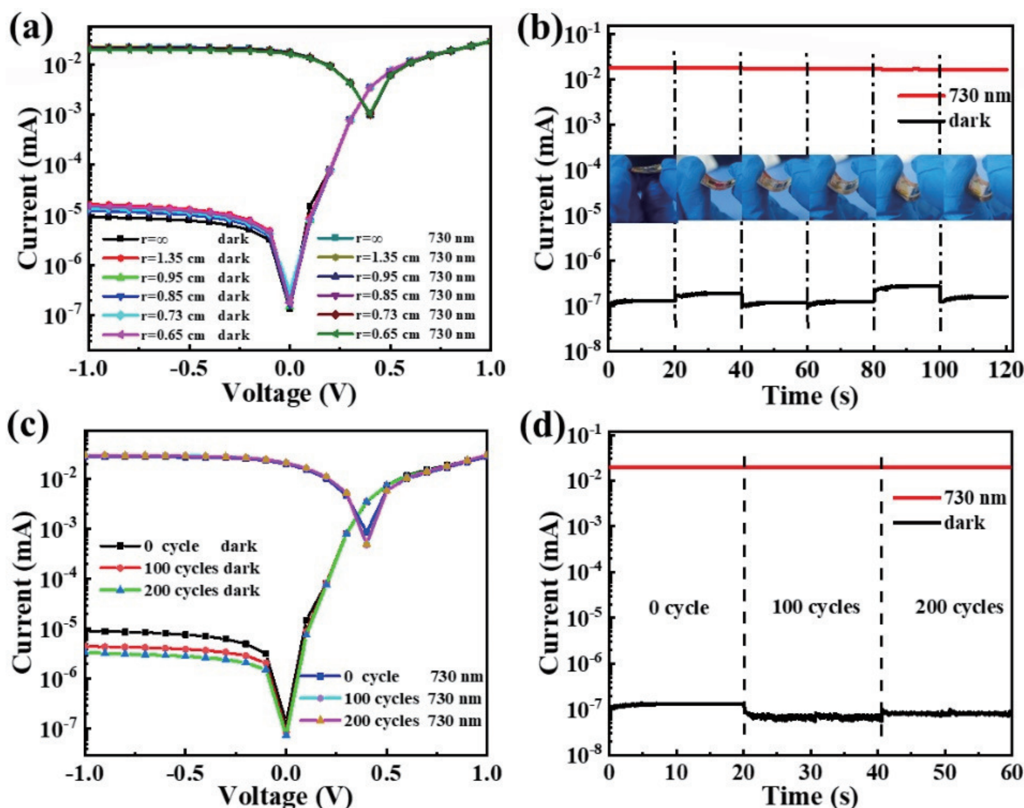

Fig. 6. (Color online) (a) *I–V* curves and (b) dark current and photocurrent of the heterostructure-based flexible light detector under different bending radii of curvature. (c) *I–V* curves and (d) photocurrent and dark current of the heterostructure-based flexible light detector before and after 100 and 200 cycles of bending tests.

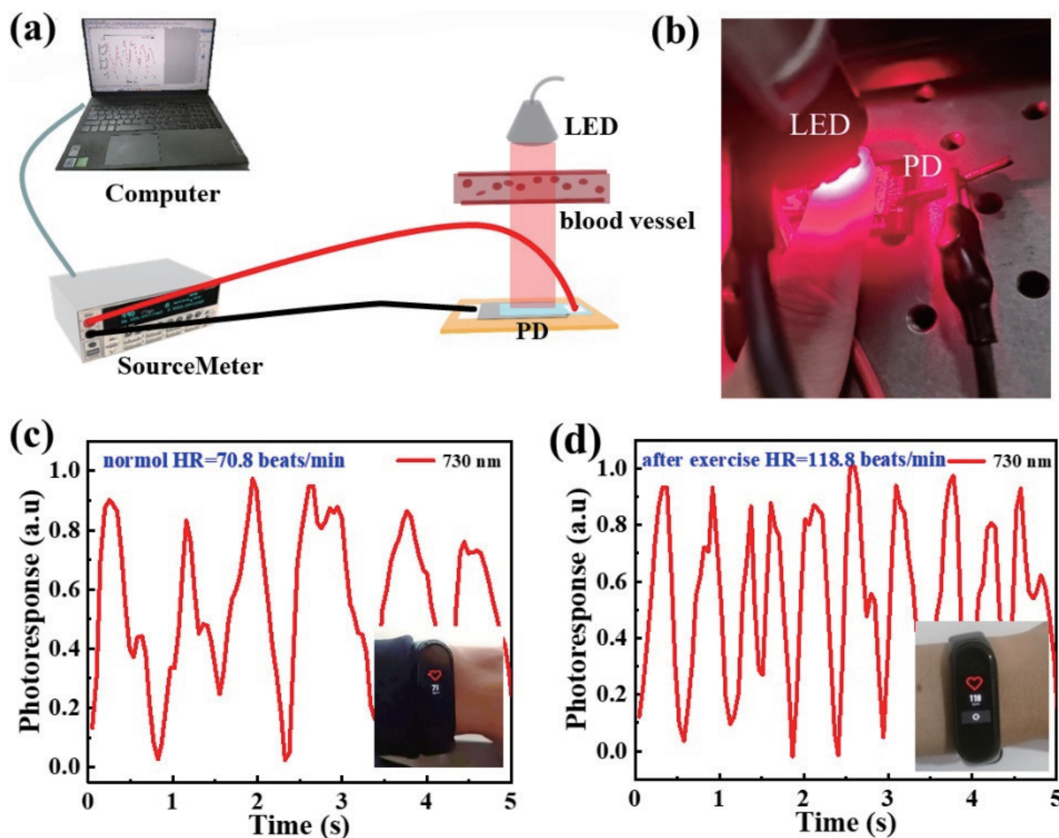

Fig. 7. (Color online) (a) Schematic diagram and (b) experimental setup of the HR detection system. LED and PD represent light emitting diode and photodetector, respectively. Normalized transient photoresponse of the heterostructure (c) at normal and (d) after exercise conditions (upon 730 nm light illumination). Insets in (c) and (d) are photographs of a commercial Mi smart bracelet, showing HR measurement results at normal and after exercise statuses, respectively.

ing 60 s using the average interbeat interval of both cases. It was found that the obtained HR values at both conditions were well coincident with the recording values of a commercial Mi smart bracelet (71 and 118 beats/min, see insets in Figs. 7(c) and 7(d)), suggesting the high accuracy of the heterostructure device for HR detection. In consideration of its good flexibility, the present light detector might hold good prospects for use in flexible and even wearable health monitoring devices.

3. Conclusions

In conclusion, we have demonstrated the construction of a highly efficient self-powered flexible photodetector by combing a $PdTe_2$ multilayer with a thin Si film. The as-fabricated heterostructure exhibited a wideband photoresponse covering the wavelength spectrum of the visible-NIR regions with current on/off ratio, responsivity, specific detectivity, and response speed attaining 10^5, ~343 mA/W, 2.56×10^{12} Jones, and 4.5/379 μs, respectively, upon 730 nm light irradiation at zero bias. In addition, the heterostructure light detector possessed excellent flexibility, robust operational durability, and long-term air stability. The outstanding photoresponse characteristics also endowed the device with good HR detection functionality. The present flexible light detector might find important applications in flexible and even wearable health monitoring devices.

Acknowledgements

This work was financially supported by the National Natural Science Foundation of China (NSFC, Nos. 62275002, 51902078, 62074048, 62075053), the Anhui Provincial Natural Science Foundation (2008085MF205), and the Fundamental Research Funds for the Central Universities (JZ2020HGTB0051, PA2020GDKC0024).

Appendix A. Supplementary materials

Supplementary materials to this article can be found online at https://doi.org/10.1088/1674-4926/44/11/112001.

References

[1] Koppens F H L, Mueller T, Avouris P, et al. Photodetectors based on graphene, other two-dimensional materials and hybrid systems. Nature Nanotech, 2014, 9, 780
[2] Buscema M, Island J O, Groenendijk D J, et al. Photocurrent generation with two-dimensional van der Waals semiconductors. Chem Soc Rev, 2015, 44, 3691
[3] Long M S, Wang P, Fang H H, et al. Progress, challenges, and opportunities for 2D material based photodetectors. Adv Funct Mater, 2019, 29, 1803807
[4] Fang H H, Hu W D. Photogating in low dimensional photodetectors. Adv Sci, 2017, 4, 1700323
[5] Xie C, Yan F. Flexible photodetectors based on novel functional materials. Small, 2017, 13, 1701822
[6] Lou Z, Shen G. Flexible photodetectors based on 1D inorganic nanostructures. Adv Sci, 2016, 3(6), 2198
[7] Ren A B, Yuan L M, Xu H, et al. Recent progress of III–V quantum dot infrared photodetectors on silicon. J Mater Chem C, 2019, 7, 14441
[8] Wu J H, Lu Y H, Feng S R, et al. The interaction between quantum dots and graphene: The applications in graphene-based solar cells and photodetectors. Adv Funct Mater, 2018, 28, 1804712
[9] Zhai T Y, Li L, Ma Y, et al. One-dimensional inorganic nanostructures: Synthesis, field-emission and photodetection. Chem Soc Rev, 2011, 40, 2986
[10] Zhai T Y, Fang X S, Li L, et al. One-dimensional CdS nanostructures: Synthesis, properties, and applications. Nanoscale, 2010, 2, 168
[11] Jie J S, Zhang W J, Bello I, et al. One-dimensional II–VI nanostructures: Synthesis, properties and optoelectronic applications. Nano Today, 2010, 5, 313
[12] Xie C, Mak C, Tao X M, et al. Photodetectors based on two-dimensional layered materials beyond graphene. Adv Funct Mater, 2017, 27, 1603886
[13] Pi L J, Li L, Liu K L, et al. Recent progress on 2D noble-transition-metal dichalcogenides. Adv Funct Materials, 2019, 29, 1904932
[14] Liu C Y, Guo J S, Yu L W, et al. Silicon/2D-material photodetectors: From near-infrared to mid-infrared. Light Sci Appl, 2021, 10, 123
[15] Yao J D, Yang G W. 2D material broadband photodetectors. Nanoscale, 2020, 12, 454
[16] Tian W, Zhou H P, Li L. Hybrid organic-inorganic perovskite photodetectors. Small, 2017, 13, 1702107
[17] Wang H, Kim D H. Perovskite-based photodetectors: Materials and devices. Chem Soc Rev, 2017, 46, 5204
[18] Xie C, Liu C K, Loi H L, et al. Perovskite-based phototransistors and hybrid photodetectors. Adv Funct Mater, 2020, 30, 1903907
[19] Yan Z H, Yang H, Yang Z, et al. Emerging two-dimensional tellurene and tellurides for broadband photodetectors. Small, 2022, 18, 2200016
[20] Zhao Y D, Qiao J S, Yu Z H, et al. High-electron-mobility and air-stable 2D layered $PtSe_2$ FETs. Adv Mater, 2017, 29, 1604230
[21] Yu X C, Yu P, Wu D, et al. Atomicallythin noble metal dichalcogenide: A broadband mid-infrared semiconductor. Nat Commun, 2018, 9, 1545
[22] Li L, Wang W K, Chai Y, et al. Few-layered PtS_2 phototransistor on h-BN with high gain. Adv Funct Mater, 2017, 27, 1701011
[23] Liang Q J, Wang Q X, Zhang Q, et al. High-performance, room temperature, ultra-broadband photodetectors based on air-stable $PdSe_2$. Adv Mater, 2019, 31, 1807609
[24] Guo C, Hu Y B, Chen G, et al. Anisotropic ultrasensitive $PdTe_2$-based phototransistor for room-temperature long-wavelength detection. Sci Adv, 2020, 6, eabb6500
[25] Li Z X, Ran W H, Yan Y X, et al. High-performance optical noncontact controlling system based on broadband $PtTe_x$/Si heterojunction photodetectors for human–machine interaction. InfoMat, 2022, 4, e12261
[26] Yim C, McEvoy N, Riazimehr S, et al. Wide spectral photoresponse of layered platinum diselenide-based photodiodes. Nano Lett, 2018, 18, 1794
[27] Wu D, Guo J W, Du J, et al. Highly polarization-sensitive, broadband, self-powered photodetector based on graphene/$PdSe_2$/germanium heterojunction. ACS Nano, 2019, 13, 9907
[28] Zeng L H, Wu D, Lin S H, et al. Photodetectors: Controlled synthesis of 2D palladium diselenide for sensitive photodetector applications. Adv Funct Mater, 2019, 29, 1970005
[29] Luo L B, Wang D, Xie C, et al. $PdSe_2$ multilayer on germanium nanocones array with light trapping effect for sensitive infrared photodetector and image sensing application. Adv Funct Mater, 2019, 29, 1900849
[30] Chen C, Li K H, Li F, et al. One-dimensional Sb_2Se_3 enabling a highly flexible photodiode for light-source-free heart rate detection. ACS Photonics, 2020, 7, 352
[31] Xu Y J, Shen H L, Li Y F, et al. Self-powered and fast response MoO_3/n-Si photodetectors on flexible silicon substrates with

light-trapping structures. ACS Appl Electron Mater, 2022, 4, 4641
[32] Ruan K Q, Ding K, Wang Y M, et al. Flexible graphene/silicon heterojunction solar cells. J Mater Chem A, 2015, 3, 14370
[33] Liang Y, Xie C, Dong C Y, et al. Electrically adjusted deep-ultraviolet/near-infrared single-band/dual-band imaging photodetectors based on $Cs_3Cu_2I_5/PdTe_2$/Ge multiheterostructures. J Mater Chem C, 2021, 9, 14897
[34] Tong X-W, Fan M, Xie C, Wang L, et al. A self-driven wideband wavelength sensor based on an individual $PdTe_2$/Thin Si/$PdTe_2$ heterojunction. J Mater Chem C, 2022, 10, 14334
[35] D'Olimpio G, Guo C, Kuo C N, et al. $PdTe_2$ transition-metal dichalcogenide: Chemical reactivity, thermal stability, and device implementation. Adv Funct Mater, 2020, 30, 1906556
[36] Li E, Zhang R Z, Li H, et al. High quality $PdTe_2$ thin films grown by molecular beam epitaxy. Chin Phys B, 2018, 27, 086804
[37] Wu E, Wu D, Jia C, et al. In situ fabrication of 2D WS_2/Si type-II heterojunction for self-powered broadband photodetector with response up to mid-infrared. ACS Photonics, 2019, 6, 565
[38] Li X M, Zhu M, Du M D, et al. High detectivity graphene-silicon heterojunction photodetector. Small, 2016, 12, 595
[39] Wang L, Jie J S, Shao Z B, et al. MoS_2/Si heterojunction with vertically standing layered structure for ultrafast, high-detectivity, self-driven visible-near infrared photodetectors. Adv Funct Mater, 2015, 25, 2910
[40] Zeng L H, Wu D, Jie J S, et al. Mid-infrared photodetectors: Van der waals epitaxial growth of mosaic-like 2D platinum ditelluride layers for room-temperature mid-infrared photodetection up to 10.6 μm. Adv Mater, 2020, 32, 2070394
[41] An X H, Liu F Z, Jung Y J, et al. Tunable graphene–silicon heterojunctions for ultrasensitive photodetection. Nano Lett, 2013, 13, 909
[42] Xie C, Wang Y, Zhang Z X, et al. Graphene/semiconductor hybrid heterostructures for optoelectronic device applications. Nano Today, 2018, 19, 41
[43] García de Arquer F P, Armin A, Meredith P, et al. Solution-processed semiconductors for next-generation photodetectors. Nat Rev Mater, 2017, 2, 16100
[44] Gong X, Tong M H, Xia Y J, et al. High-detectivity polymer photodetectors with spectral response from 300 nm to 1450 nm. Science, 2009, 325, 1665
[45] Xiao P, Mao J, Ding K, et al. Solution-processed 3D RGO-MoS_2/pyramid Si heterojunction for ultrahigh detectivity and ultra-broadband photodetection. Adv Mater, 2018, 30, 1801729
[46] Li J H, Niu L Y, Zheng Z J, et al. Photosensitive graphene transistors. Adv Mater, 2014, 26, 5239
[47] Yao J D, Zheng Z Q, Yang G W. Production of large-area 2D materials for high-performance photodetectors by pulsed-laser deposition. Prog Mater Sci, 2019, 106, 100573
[48] Palik E D, Glembocki O J, Heard I Jr, et al. Etching roughness for (100) silicon surfaces in aqueous KOH. J Appl Phys, 1991, 70, 3291
[49] Lochner C M, Khan Y, Pierre A, et al. All-organic optoelectronic sensor for pulse oximetry. Nat Commun, 2014, 5, 5745
[50] Xu H H, Liu J, Zhang J, et al. Flexible organic/inorganic hybrid near-infrared photoplethysmogram sensor for cardiovascular monitoring. Adv Mater, 2017, 29, 1700975

Chengyun Dong got his BS degree from Anhui Polytechnic University in 2020. Now he is a master student at School of Microelectronics, Hefei University of Technology, under the supervision of Prof. Linbao Luo. His research focuses on two-dimensional layered materials and optoelectronic devices.

Chao Xie received his doctoral degree from Hefei University of Technology, Hefei, China, in 2014. He is currently a Professor with Industry-Education-Research Institute of Advanced Materials and Technology for Integrated Circuits, Anhui University, Hefei, China. His current research focuses on development of high-performance optoelectronic devices based on novel functional materials.

Linbao Luo received his doctoral degree from City University of Hong Kong in 2009. He is currently a Professor with School of Microelectronics, Hefei University of Technology, Hefei, China. He has long been engaged in the research of high-performance optoelectronic devices and optoelectronic integration technology based on new semiconductor materials.